Journal of Hydrology 625 (2023) 130061

Contents lists available at ScienceDirect

Journal of Hydrology

journal homepage: www.elsevier.com/locate/jhydrol

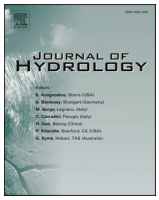

Research papers

Characterizing basin-scale subsurface hydraulic heterogeneity with multiscale geological and hydrological measurements

Hong-Ru Lin [a], Jet-Chau Wen [b,c], Zaiyong Zhang [d,e], Yu-Li Wang [f,*]

[a] Graduate School of Engineering Science and Technology, National Yunlin University of Science and Technology, Taiwan
[b] Department of Safety, Health and Environmental Engineering, National Yunlin University of Science and Technology, Taiwan
[c] Research Center for Soil and Water Resources and Natural Disaster Prevention, National Yunlin University of Science and Technology, Taiwan
[d] Key Laboratory of Subsurface Hydrology and Ecological Effects in Arid Region, Chang'an University, Ministry of Education, China
[e] School of Water and Environment, Chang'an University, China
[f] Department of Bioenvironmental Systems Engineering, National Taiwan University, Taiwan

ARTICLE INFO

This manuscript was handled by Corrado Corradini, Editor-in-Chief, with the assistance of Nick Engdahl, Associate Editor

ABSTRACT

Mapping aquifer heterogeneity is a pressing need for managing regional groundwater resources. Many studies have shown that combining hydraulic tomographic surveys with point-scale geological information is viable for detailing meter-scale to kilometer-scale hydraulic heterogeneity of aquifers. However, due to the complexity of aquifer systems, few field investigations have been conducted on basin-scale systems. In this study, we collected datasets of stream stages, groundwater levels, and borehole logs from 35 wells in a river plain during the wet season, when flood events altered the groundwater flow fields. We then analyzed these datasets using correlation analysis and a geostatistical inverse model. The hydraulic transmissivity and storage coefficient distributions were inverted based on different numbers of geological zones. By validating the estimated parameter fields with independent datasets, we demonstrated that appropriate selection of the number of geological zones, using point-scale geological information and clustering, improved the estimated fields. Further increasing the number of zones beyond an appropriate number deteriorated the estimates at the basin-scale site. The proposed method offers a cost-effective approach for basin-scale characterization. The better knowledge of subsurface hydraulic heterogeneity can support water resource management decisions.

1. Introduction

High-resolution characterization of subsurface hydraulic characteristics is crucial for managing, conserving, and protecting groundwater resources at the scale of our interests (Yeh et al., 2023). Properties like permeability and specific storage of the subsurface affect the movement of groundwater, which impacts the rate and direction of groundwater flow and migration of hazardous and valuable chemicals in the aquifer. Accurate mapping the distributions of these properties can assist in developing effective groundwater management strategies, including identifying potential contamination sources or optimizing the remediation wells' placement. The presence of fractures, faults, and other geological structures can also significantly affect water flow and contaminant migration through the subsurface. Additionally, certain types of soils and rocks may be more prone to retaining or spreading contaminants. As such, characterizing these properties with high spatial resolution can improve our strategies for preventing or mitigating contamination.

Many studies have emphasized the importance of site-specific heterogeneity among the various factors contributing to the effectiveness of aquifer management. For instance, Hartmann et al. (2017) reported that aquifer heterogeneity determines the groundwater recharge rate and its sensitivity to climate variability. Sarris et al. (2022) suggested that when the number of monitoring wells is limited, contaminant detection rates are higher when the heterogeneity is greater. Michael and Khan (2016) stressed that while heterogeneous and equivalent homogeneous simulations produce similar management insights, the spatial distribution of properties and their correlation can significantly affect solute transport rates and directions relative to equivalent homogeneous systems. Luo et al. (2020) interpreted the long-term water-supply pumping/injection records and showed the importance of inter/intra-layer heterogeneity in predicting solute transport in a synthetic multi-aquifer/aquitard system.

* Corresponding author.
E-mail address: ylwang@ntu.edu.tw (Y.-L. Wang).

https://doi.org/10.1016/j.jhydrol.2023.130061
Received 8 May 2023; Received in revised form 27 June 2023; Accepted 1 August 2023
Available online 10 August 2023
0022-1694/© 2023 Elsevier B.V. All rights reserved.

For these reasons, an intelligent groundwater resources monitoring and management framework was suggested considering a detailed hydrogeology characterization (Hoffman, 1993; Yeh et al., 2008; Yeh et al., 2023).

While various aquifer characterization methods exist, characterizing subsurface hydraulic heterogeneity through river stage variation is a technique that is currently being developed. This method is based on the joint interpretation of non-fully-redundant information about aquifer heterogeneity carried by the groundwater variation fields induced by the river stage variations during the propagation of a flood wave from upstream to downstream (Yeh et al., 2009). The flood wave generates different flow fields, each of which reflects the heterogeneity in certain parts of the aquifer from a specific perspective. Field investigations have revealed that the pressure responses of aquifers due to river excitations can propagate for several kilometers or more than ten kilometers in confined or semi-confined aquifers, with fluctuations ranging from a few centimeters to meters (Sophocleous, 1991; Promma et al., 2007; Jardani et al., 2012; Ramirez-Hernandez et al., 2013; Hsiao et al., 2017; Wang et al., 2017).

Over the past few decades, the potential of river stage variation for subsurface characterization has been widely recognized. Yeh et al. (2009) demonstrated the potential of river stage tomography in synthetic stream-aquifer systems using event-based flood waves. Jardani et al. (2012) inverted the transmissivity field of a heterogeneous alluvial aquifer along a tidal river. Wang et al. (2017) used seasonal river stage variations as excitation sources to characterize an alluvial fan with complex hydrogeological structures. The resolution of estimates is influenced by the time scales of the river stage variation, and Wang et al. (2019) further investigated the different forms of river stage fluctuation. They suggested that, if noise levels are similar, event-based flood waves are better than long-term periodic excitations.

The basin-scale sites usually have geological maps that provide the distribution of different types of rock and surficial deposits, as well as the locations of geologic structures such as faults and folds. Practitioners typically use these geological data obtained from boreholes and outcrops to build conceptual models (Troldborg et al., 2007; Refsgaard et al., 2012; Enemark et al., 2019; Jafarzadeh et al., 2022). In this traditional approach, the area of interest is divided into several hydrogeological zones based on available geological data, such as outcrops, geological maps, and borehole logs, and homogeneous hydraulic parameters are assumed throughout each zone. While the approach may be practical, inaccurate geological information leads to persistent discussions about the structural adequacy (Gupta et al., 2012) and the necessity to evaluate alternative models (Troldborg et al., 2007; Refsgaard et al., 2012; Schöniger et al., 2015).

To address the large-scale geologic features, Liu and Oliver (2005) used the ensemble Kalman filter to adjust facies boundaries to match production data. A level set method and total variation prior Bayesian inversion were proposed by Cardiff and Kitanidis (2009), Lee and Kitanidis (2013), and Iglesias et al. (2016) to identify the boundaries between large-scale geologic structures. The level set method is flexible to map geologic structure boundaries in any shape, size, or number. While these methods are general for facies-dominated problems, the small-scale heterogeneity within each geologic structure and its impact on the facies identification were not contemplated.

Advances have been made to develop methods for including qualitative geological data while considering the within zone variability. The geological data can be collected using core samples (Zhao et al., 2016) or inferred using well logging tools such as Hydraulic profiling tool (Zhao and Illman, 2022). Zhao et al. (2016) demonstrated that when calibrating steady-state groundwater models with varying subsurface conceptualizations and parameter resolutions, the highly parameterized geostatistical inversion approach with a geological model as prior information performed the best. The performance of high-resolution geostatistical models with uniform prior mean was slightly worse. Subsequently, improved accuracy and resolution of estimated hydraulic parameter fields have been observed through transient-state studies in a sandbox (Luo et al., 2017), meter-scale research sites (Zhang et al., 2016; Zhao and Illman, 2018; Zhao and Illman, 2022), and kilometer-scale field sites (Zha et al., 2019; Luo et al., 2022). Only a few tomographic surveys have been demonstrated in basin-scale systems (i.e., tens of kilometers or more) where hydraulic parameter distributions are estimated based on sparse prior geological datasets.

The objective of this study focuses on assessing the importance and potential of including sparse geological information in a basin-scale groundwater model inversion, where the boundaries of different types of depositions are suspected and uncertain. We intend to (1) demonstrate the application of integrating existing multiscale datasets to identify subsurface features at a tens of kilometers scale aquifer system and (2) investigate the optimal number of zones used in the prior model for the basin-scale investigation. To achieve these goals, we acquired historical groundwater level data from a plain where many individual flood waves along the rivers are generated by heavy rainfalls. Additionally, we obtained geological borehole log data from the site. With these datasets, we expect to demonstrate that the groundwater level responses induced by changes in stream stages contain valuable information about aquifer heterogeneity. Proper analysis of the datasets using a highly parameterized geostatistical inverse model with the aid of available geological information from the boreholes could yield high-resolution maps of hydraulic parameters, such as transmissivity (T) and storage coefficient (S) of the field site.

2. Site descriptions

2.1. Topography

The Pingtun Plain is located in southern Taiwan, approximately 25 km in width and 60 km in length, with an area of 1,200 km^2 (Fig. 1a). It is surrounded by foothills and river valleys (Alishan Mountain Range) to the north, Lingkou Hills to the west, the Taiwan Strait to the south, and the Central Mountain Range and Chaochou Fault to the east. Three major rivers, the Gaoping River, Donggang River, and Linbian River, flow through the plain from northeast to southwest and discharge into the Taiwan Strait. The elevation gradually decreases from 200 m above the sea level towards the southwest coast. Groundwater levels are 45 m below the ground near the mountain front and only a few meters below the ground surface in the southwest part of the plain.

2.2. Geology

The geological profiles (Fig. 1b), inferred from well logs, reveal at least three aquifers over a depth of 220 m (Central Geological Survey, 1994). These aquifers are connected to each other at the north and east parts of the plain, where deposition is mainly gravel (as shown in blue zones in Fig. 1b). The middle and tail of the plain consist of non-marine deposit gravel and sandy aquifers. They are separated by the aquitards (as shown in yellow zones in Fig. 1b), characterized as marine deposition due to abundant fossils such as shells and foraminifera. The aquitards pinch out in the upstream and mountain front regions. These geologic features reflect the rising and falling of the mean sea levels caused by global climate change late in the Quaternary Period. The sediment distribution in the plain follows a gravel, sand, and clay pattern from the top to the tail of the plain. This pattern is consistent with the river deposition process: angular conglomerates and breccias settle down first at the headwater where transport energy is high, while the arkose and finer materials, such as silt and clay, are precipitated at the middle and tail of the river, where transport energy is low or even transported further into the ocean.

The hydraulic conductivity values of each aquifer are primarily between 1 and 10 m/day, with values gradually decreasing from the northeast to the southwest as they approach the shoreline. The top aquifer is more permeable than the second and third aquifers. The top

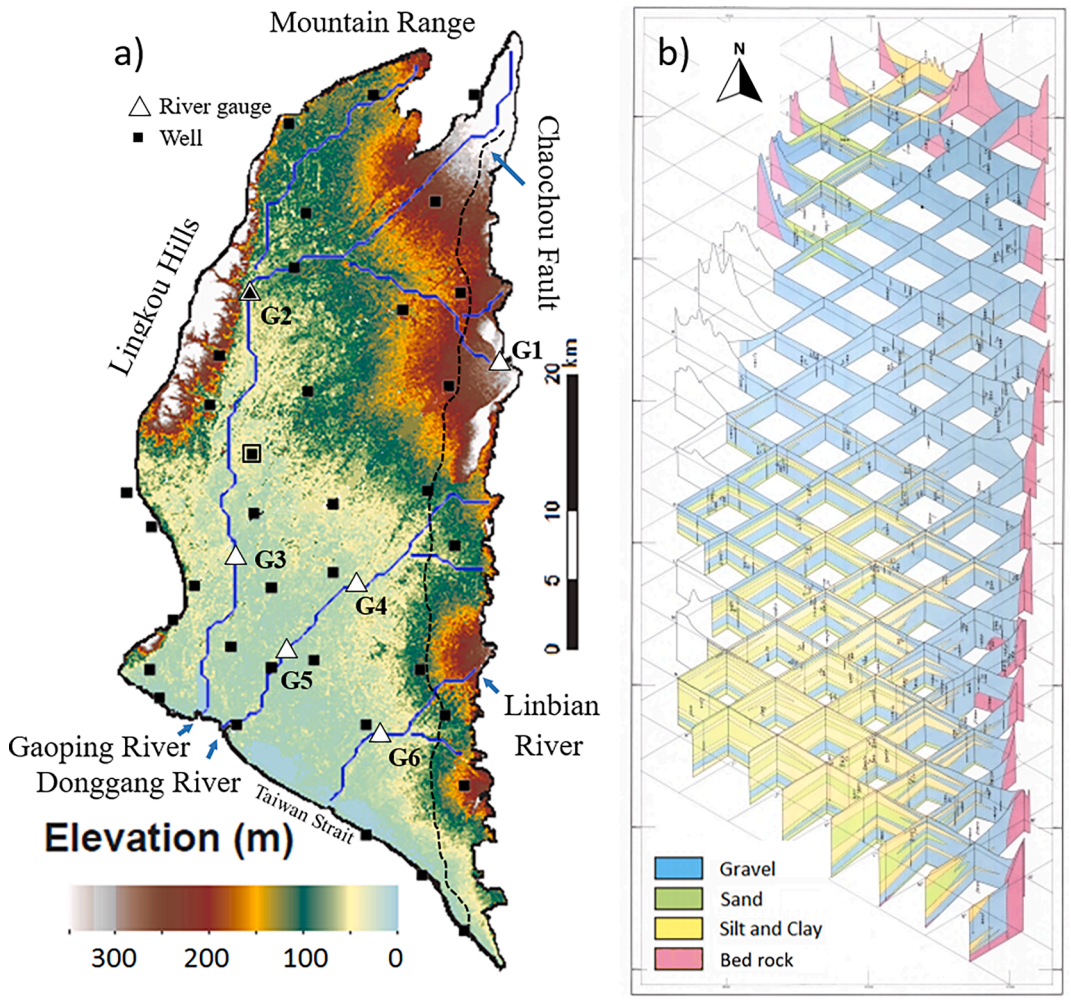

Fig. 1. a) topography of the study plain. the blue lines represent rivers, the black squares are groundwater monitoring wells, and the white triangles indicate the stream gauge stations. b) the geological profiles based on core samples (figure adapted from Central Geological Survey, 1994). (For interpretation of the references to color in this figure legend, the reader is referred to the web version of this article.)

aquifer is more than 150 m thick in the upstream and mountain front regions where three aquifers are connected. The thickness of the top aquifer gradually decreases to around 30 m towards the shoreline. The thickness of the second aquifer is around 10 to 80 m and that of the third aquifer is about 50 to 90 m. These three aquifers span across the entire plain.

2.3. Hydrological data availability

The groundwater monitoring network comprises 60 evenly distributed groundwater stations, with more than 130 monitoring wells installed at depths ranging from 10 to 200 m. Most of the wells are screened at a single depth. For this study, 35 monitoring wells were selected. The remaining wells are excluded because their screen intervals are opened at the second and third aquifers. The screen intervals of selected wells were opened at the unconfined or partially confined aquifer, mostly ranging from 15 to 40 m below the surface. The wells located at the north and east parts of the plain or near the mountain front may have openings at depths up to 100 m below the surface. The water levels are recorded hourly.

There are three stream gauging stations (white triangles), one at the top (G1), one in the middle (G2), and one at the tail of the plain (G3), along the Gaoping River, namely Tjimur, Liling Bridge, and Wanda Bridge, respectively. Two stream gauging stations, Teochew (G4) and Gangdong No. 2 Bridge (G5), are located along the Donggang River at the middle and tail of the plain. The Xinpi gauging station (G6) at the midstream of the Linbian River provides additional data on river flow in the southeast corner of the plain. The river stage and flow rate are recorded hourly.

The selected daily stream stages, flow rates, and groundwater levels

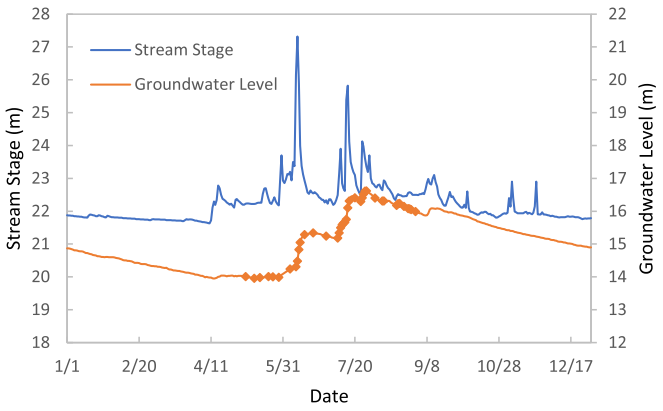

Fig. 2. The stream stage variations (at the concentric triangle (G2) in Fig. 1a) and groundwater level variations during 2006 (at the concentric square in Fig. 1a). The groundwater level station is 2.5 km away from the river's main channel.

(markers in Fig. 2) are used to explore the hydrological processes and subsurface heterogeneity in the Pingtun Plain. The data are chosen to minimize storage requirements during inversion while preserving stream stage and groundwater level fluctuations. Fig. 2 shows the time series of stream stage (concentric triangle, G2) and groundwater level variations (concentric square, 2.5 km away from the river's main channel) from 1/1 to 12/31, 2006, which reveal their significant correlation during the rainfall season from May to October 2006. The rising and falling trends in groundwater levels are consistent with but lag behind the river stage fluctuations. Also, the groundwater fluctuations are smoother than the river stage. Other stream stage and groundwater level fluctuations are presented in Fig. S1.

3. Methods

While Fig. 2 illustrates that the groundwater fluctuations correspond to the river stage variations, many natural processes (e.g., precipitation, mountain front recharge) or human activities (e.g., pumping and irrigation) at different time scales and frequencies may induce similar responses in the groundwater level. Differentiating the effects of various excitations on groundwater level signals is necessary for this study. Because of the lack of comprehensive data and knowledge of all the natural processes and human activities, correlation analysis is employed to study the temporal variation of river stage and groundwater data, allowing us to identify the most suitable time period where the relationship between the two variables is most significant. Afterward, we use a geostatistical algorithm and the river stage and groundwater data to estimate T and S distributions in the plain. This section briefly discusses the correlation analysis, the k-means++ clustering, and the Successive Linear Estimator (see Fig. 3 for the flow chart).

3.1. Groundwater flow and river models

The 2-D groundwater flow in a heterogeneous confined aquifer is described as

$$\nabla\cdot[T(\mathbf{x})\nabla h(\mathbf{x},t)] = S(\mathbf{x})\frac{\partial h(\mathbf{x},t)}{\partial t} \tag{1}$$

subject to the initial and boundary conditions

$$h|_{\Gamma_1} = h(\mathbf{x},t)h = h(\mathbf{x},t_0) \tag{2}$$

where h is the head responses (L), T is the hydraulic transmissivity (L^2/T), S is the storage coefficient (-), $\mathbf{x}$ is the vector in x and y directions, t represents time (T), and Γ_1 is the prescribed head at the Dirichlet boundary.

The linearized diffusion wave equation is employed to describe the movement of a flood wave as it propagates downstream. The equation is a simplified form of the Saint-Venant equations. It is derived from the continuity and momentum equations that govern the flow of water in a channel (Yen and Tsai, 2001).

$$D\frac{\partial^2 h(x,t)}{\partial x^2} - c\frac{\partial h(x,t)}{\partial x} = \frac{\partial h(x,t)}{\partial t} \tag{3}$$

in which D is the generalized hydraulic diffusivity (L^2/T) and c is the wave celerity (L/T).

Since rivers are generally losing streams during the wet season in Pingtun Plain, we assume that the influence of the aquifer on stream flow is negligible. Hence, we use a one-way coupling scheme to incorporate the river into the groundwater flow model, which helps to reduce the computational cost of a fully-coupled model. Specifically, the diffusion wave equation is first employed to simulate the stream stages along the river based on the observed river stage or flow rate. Afterward, the resulting stream stages were used as the prescribed heads along the river in the groundwater flow model.

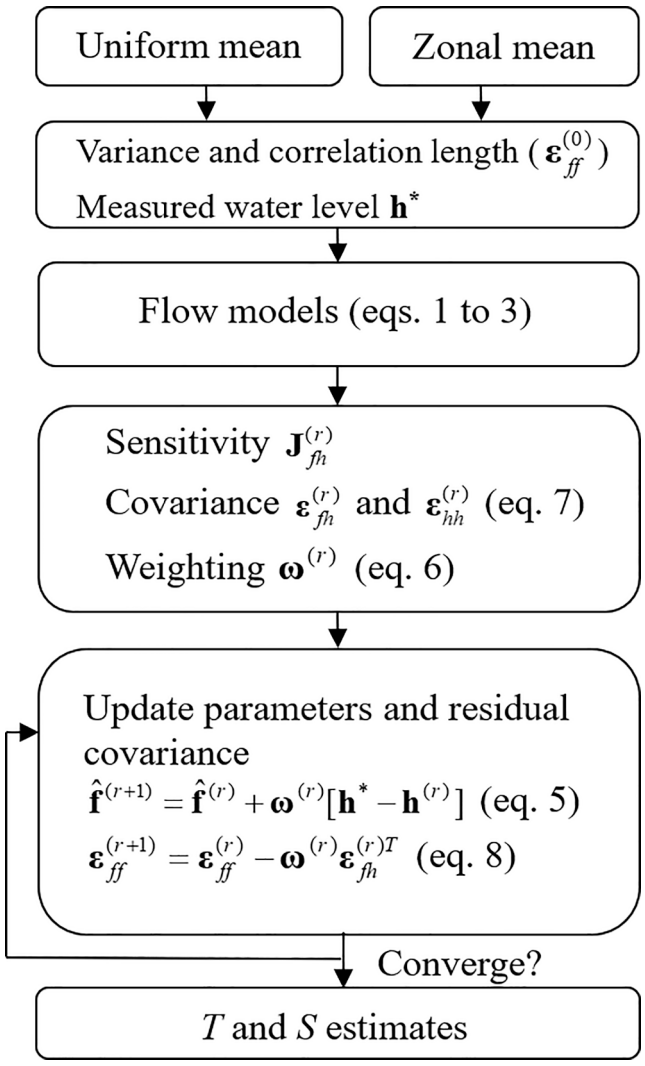

Fig. 3. The flowcharts of Successive Linear Estimator, SLE.

3.2. Spatial correlation analysis

Cross-correlation is a statistical analysis that quantifies the similarity of two time series as a function of the time lag of one relative to the other. The analysis plays a critical role as it serves two important purposes. Firstly, it helps to confirm whether the river stage influences significant changes in groundwater levels during flood events. Such knowledge is crucial for understanding the complex interactions between surface water and groundwater systems and predicting groundwater response to changes in the river stage. Secondly, the spatial patterns of correlation can confirm whether they reflect the known geological structure of the study area. In other words, a better understanding of the hydrological system can be achieved by cross-validating the results of spatial correlation analysis with geological surveys.

The correlation between river stage at different gauging stations and groundwater fluctuation at each individual well is evaluated by:

$$Cor(\tau) = \sum\frac{[h_1(t)-\overline{h}_1][h_2(t-\tau)-\overline{h}_2]}{\sigma_{h1}\sigma_{h2}} \tag{4}$$

where Cor(τ) is the cross-correlation (-), τ is the time lag or sampling point lag (T), and h_1 and h_2 represent the time series of stream stage (L) and groundwater level (L), respectively. The overbar represents the mean, and σ is the standard deviation of the corresponding time series. After establishing these correlations, they are interpolated and

extrapolated using ordinary kriging to the entire plain. The exponential variogram is used. The correlation lengths of all directions are 20 km.

3.3. K-means++ Clustering

The K-Means++ clustering algorithm (Arthur and Vassilvitskii, 2007) partitions a dataset into groups based on the similarity between data points in the same group and dissimilarity to data points in other groups based on the Euclidean distance or any other appropriate distance metric. This method can be used to define the geological formation because it consists of similar physical characteristic that distinguishes a formation from adjacent subsurface in a geographical region.

The algorithm consists of four steps. First, randomly select one data point from the dataset as the first centroid. Second, calculate each points' distance to the nearest centroid. Third, select the next centroid from the remaining data points with a probability proportional to the square of the calculated distance, which ensures that points farther away from the existing centroids are more likely to be chosen as new centroids. Repeat the second and third step until k centroids have been selected. Fourth, assign data points to the nearest centroid. This algorithm is more likely to be well-spaced and representative of the underlying data distribution than the original k-mean algorithm. It reduces the chances of converging to suboptimal solutions and improves the overall performance.

3.4. Successive linear estimator (SLE)

The successive linear estimator (Yeh et al., 1996; Xiang et al., 2009) is a powerful tool for estimating subsurface hydraulic parameters and state variables based on spatial and temporal observations. This inverse algorithm considers hydraulic parameters and state variables as a spatial stochastic process characterized by statistical information such as mean, variance, and spatial correlation function. The estimated parameter field, discretized into n_f elements, is iteratively determined using a linear estimator that incorporates observed and simulated head values and the sensitivity of the observed head to the estimated parameters. The linear estimator is:

$$\widehat{\mathbf{f}}^{(r+1)} = \widehat{\mathbf{f}}^{(r)} + \boldsymbol{\omega}^{(r)}[\mathbf{h}^{*} - \mathbf{h}^{(r)}] \tag{5}$$

in which $\widehat{\mathbf{f}}$ ($n_f \times 1$) is the estimated T or S, $\mathbf{h}^{*}$ ($n_d \times 1$) is the observed head, $\mathbf{h}^{(r)}$ ($n_d \times 1$) is the simulated head based on the estimated parameters from the r^{th} iteration, n_d is the number of observations, and the superscript r is the iteration index starting from zero. $\boldsymbol{\omega}^{(r)}$ ($n_f \times n_d$) is a weighting matrix that links the heads to parameters. This weighting matrix is solved by:

$$\boldsymbol{\omega}^{(r)}[\boldsymbol{\varepsilon}_{hh}^{(r)} + \boldsymbol{\theta}^{(r)}\mathbf{I}] = \boldsymbol{\varepsilon}_{fh}^{(r)} \tag{6}$$

where $\boldsymbol{\varepsilon}_{hh}^{(r)}$ ($n_f \times n_d$) is the covariance matrix of head at r^{th} iteration and $\boldsymbol{\varepsilon}_{fh}^{(r)}$ is the covariance matrix of head to T or S. The term $\boldsymbol{\theta}^{(r)}$ is a dynamic stabilizer that ensures numerical stability of solving an inverse matrix. We utilize the Levenberg-Marquardt algorithm. $\mathbf{I}$ is the identity matrix.

The covariance matrices $\boldsymbol{\varepsilon}_{hh}^{(r)}$ and $\boldsymbol{\varepsilon}_{fh}^{(r)}$ are derived from the first-order approximation:

$$\varepsilon_{hh}^{(r)} = J_{fh}^{(r)T}\varepsilon_{ff}^{(r)}J_{fh}^{(r)} \text{ and } \varepsilon_{fh}^{(r)} = \varepsilon_{ff}^{(r)}J_{fh}^{(r)} \tag{7}$$

in which $\mathbf{J}_{fh}^{(r)}$ ($n_f \times n_d$) is the sensitivity of the head to the estimated parameters during the r^{th} iteration. It is evaluated by the adjoint approach (Sykes et al., 1985; Sun and Yeh, 1990). $\boldsymbol{\varepsilon}_{ff}^{(r)}$ ($n_f \times n_f$) is the residual covariance matrix of T or S at r^{th} iteration and is given by:

$$\varepsilon_{ff}^{(r+1)} = \varepsilon_{ff}^{(r)} - \omega^{(r)}\varepsilon_{fh}^{(r)T} \tag{8}$$

The diagonal terms of $\boldsymbol{\varepsilon}_{ff}^{(r)}$ represent the uncertainty of the parameters, while the off-diagonal terms represent the cross-covariances between parameters. They provide information about the uncertainty and correlation between the estimated parameters. At iteration $r = 0$, $\boldsymbol{\varepsilon}_{ff}^{(r)}$ is constructed based on the prior geological knowledge of T or S using variances, correlation lengths, and covariance finctions.

The iteration process terminates when the maximum iteration number is reached or when the mismatch between the simulated and observed head is smaller than a user-specified value. In summary, SLE starts with some geostatistical information on T and S parameters, including the mean, variance, and correlation scale. It then fuses the water level information by iteratively updating the conditional mean T and S fields and their covariance functions. The estimated fields, conditioned on the given datasets, are unbiased and are the most likely estimates with the smallest variance (uncertainty).

4. Spatial correlation analysis

Fig. 4a to 4e illustrate the contour maps of the cross-correlation values between the stream stage at different gauging stations and the groundwater level at all monitoring wells in the Pingtun Plain at different selected time lags. Different time lags were selected to reflect high correlation values between the stream stage at different gauging stations and the groundwater levels at all the wells.

Fig. 4a shows the contour map of correlation coefficients between groundwater levels at all observation wells and the river stage recorded at the Tjimur station (the solid triangle (G1) upstream of the Gaoping River. This map indicates that the river stage at G1 is highly correlated ($R > 0.6$) with groundwater levels along the river flow path and the eastern boundary of the plain (i.e., the Central Mountain Range and Chaochou Fault). The high correlation areas are shown in warm colors. The topographical and geological maps indicate these areas are located along the mountain front gravel deposition (blue area in Fig. 1b). Besides, the large time lags may represent the infiltration through the vadose zone along the mountain front region. On the other hand, there is no significant correlation ($R < 0.3$) between the river stage at the Tjimur station (G1) and the observation wells in the Donggang River basin and the coastal area (greenish blue areas in Fig. 4a). This result is likely indicative of a relatively low T or high S barrier blocking the pressure wave propagating from the Gaoping River to the Donggang River basin.

Fig. 4b shows a high correlation between the river stage at the midstream of Gaoping River (i.e., Liling Bridge, G2) and groundwater levels at observation wells from the north to the middle of the plain (shown in warm colors). This contour map suggests that the subsurface hydraulic characteristics in these regions are likely similar. On the other hand, the correlation between river stage variations at downstream of Gaoping River (Wanda Bridge, G3) and groundwater levels, presented in Fig. 4c, is only significant in narrow regions along the river and is less correlated with groundwater levels in the Donggang River basin (shown in green and blue colors), despite being close to the downstream of Gaoping River.

The contour maps in Fig. 4d and 4e, illustrating the correlation coefficients between groundwater levels and river stage located on the midstream and downstream of Donggang River, have similar spatial patterns as those in Fig. 4a, 4b, and 4c, except the correlations change from low to high values. Note that the groundwater level variations within the Donggang River basin are highly correlated with the Donggang River but less correlated with groundwater levels in the Gaoping River basin, indicative of some groundwater barrier between these two river valleys.

5. Field experiment

After conducting correlation analysis, we carried out a tomographic analysis using the field dataset to depict the hydraulic heterogeneity of

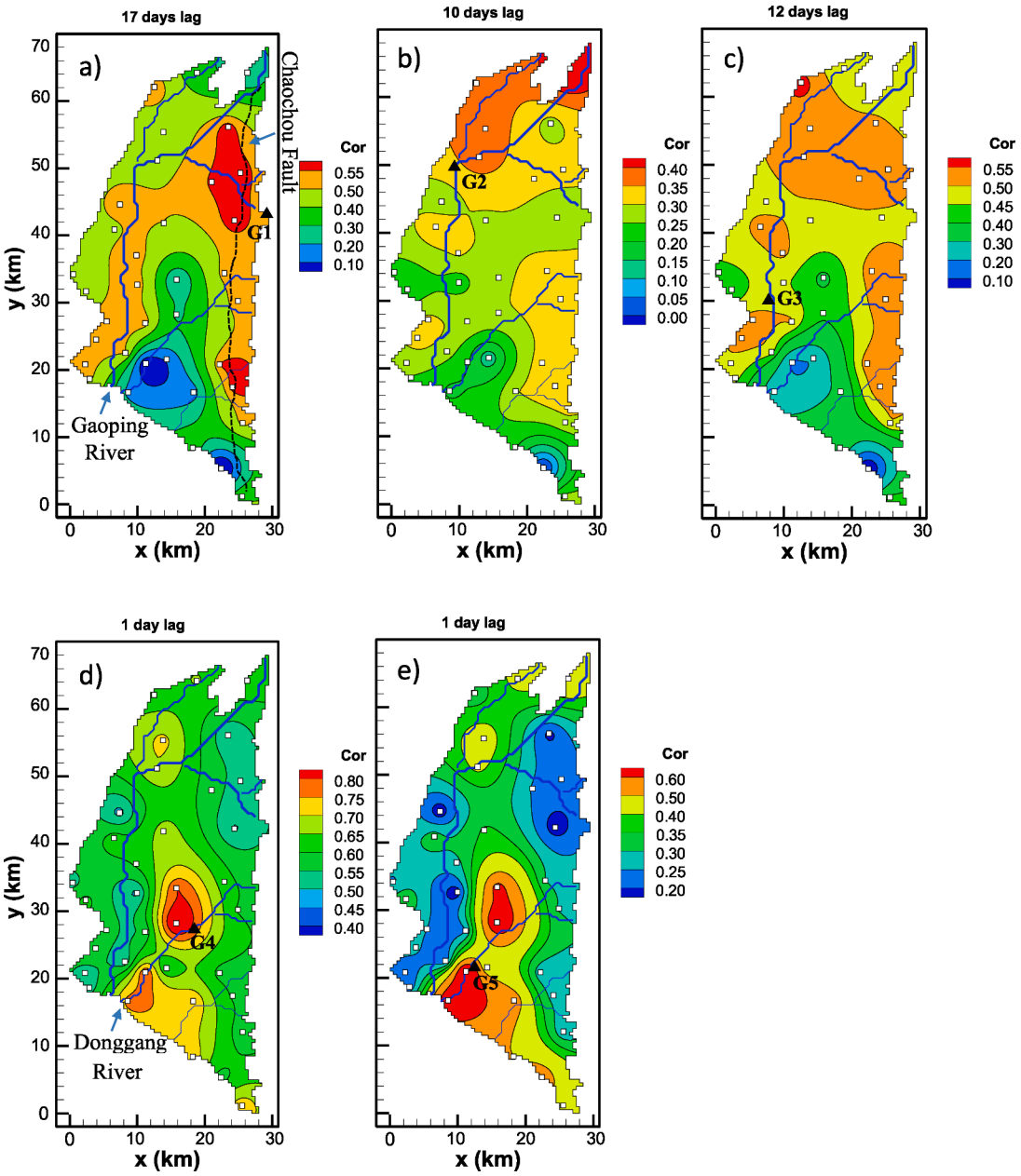

Fig. 4. The correlation contour maps at the selected time lag between the stream stage at different gauging stations (Tjimur (G1), Liling Bridge (G2), Wanda Bridge (G3), Teochew (G4), and Gangdong No. 2 Bridge (G5), respectively) and the groundwater levels at all monitoring wells. The white squares denote the wells, and the black triangles denote the stream gauge stations.

the shallow aquifer. We conducted the tomographic analysis using different prior mean hydraulic parameter values and distributions. Initially, we used uniform mean T and S values without incorporating any prior hydrogeological knowledge into the model. These parameters are effective values based on a single zone. Next, we used the calibrated mean T and S values from a calibrated zonation model as the prior mean, which involves three steps. Firstly, we utilized the datasets obtained from the Central Geological Survey (1994) to derive a kriged parameter field. These datasets included the ranges of T and S values, as well as the borehole geological data. Secondly, since the variabilities of the parameter values and their geographical positions (x and y) differ significantly in magnitude, we linearly rescaled both types of values to the range between 0 and 1. Thirdly, we created a zonation model consisting of several zones using a k-means++ clustering algorithm. The zones were clustered based on the rescaled kriged values and their rescaled geographical positions. We considered different numbers of zones (1, 2, 3, 4, 5, 6, 7, 8, and 10) and ensured that the zone patterns maintained the general structure of the site geology. Afterward, SLE estimated each zone's effective T and S values that yielded simulated heads best matched the observed head. Finally, these effective parameter values of zones serve as the prior mean to calibrate the highly parameterized model. This method aims to avoid the conceptual model surprise and unforeseen consequences of incorrect prior parameter structures in implementing inverse modeling (Bredehoeft, 2005).

We use two criteria to evaluate the inversion results. The first criterion is the scatterplot of the simulated head changes versus the observed data, using the L_2, and linear regression line's slope, intercept, and R^2. The second is to validate the estimated T and S fields by their ability to predict the head changes in the observation wells not used in the inversion.

5.1. Model layouts

The study site was discretized into 5619 grids, each measuring 0.5 km × 0.5 km. We selected groundwater level data from June to September 2006, collected from 35 monitoring wells evenly distributed throughout the catchment. We randomly selected water levels from 23 wells for model calibration, and the remaining water levels from 12 wells were used for validation. The effect of the unsaturated zone is ignored because the groundwater level fluctuations are much smaller than the aquifer thickness. To minimize the effect of mountain front lateral recharge, we used a time-varying head boundary to encircle the aquifer by extrapolating these boundary heads using kriging with data collected from all monitoring wells. The simulation domain along the coast is extended 5 km outward and is set as a zero constant head boundary.

We simulated the initial groundwater level by spinning up the model for six years before June 2006 with the mean hydraulic transmissivity (1 m^2/day), the mean storage coefficient (10^{-5}), a time-varying head boundary, and stream stage variations. These mean parameter values were chosen because the plain primarily consists of gravel and sand deposits. The process of initializing (spinning up) a numerical simulation of a groundwater flow model with a set of model parameters, initial conditions, and boundary conditions allows the simulation to run until the groundwater levels at a later time (such as June 2006) are no longer affected by uncertain initial head distributions.

The SLE algorithm requires the prior spatial statistics of the unknown ln$T$ and ln$S$ to be specified. Based on hydrogeological knowledge of the site, we set the geometric mean of T to 1 m^2/d and the mean S to 10^{-4}. We also set the variance of ln$T$ and ln$S$ to 1.0. Although these variance values were uncertain, they only had minor impacts on the parameter and uncertainty distributions because the variances exist in both the numerator and denominator in equations (4) and (5), and their effects on the estimations cancel out. We described the spatial correlation using an exponential covariance function with correlation scales of 15 km in

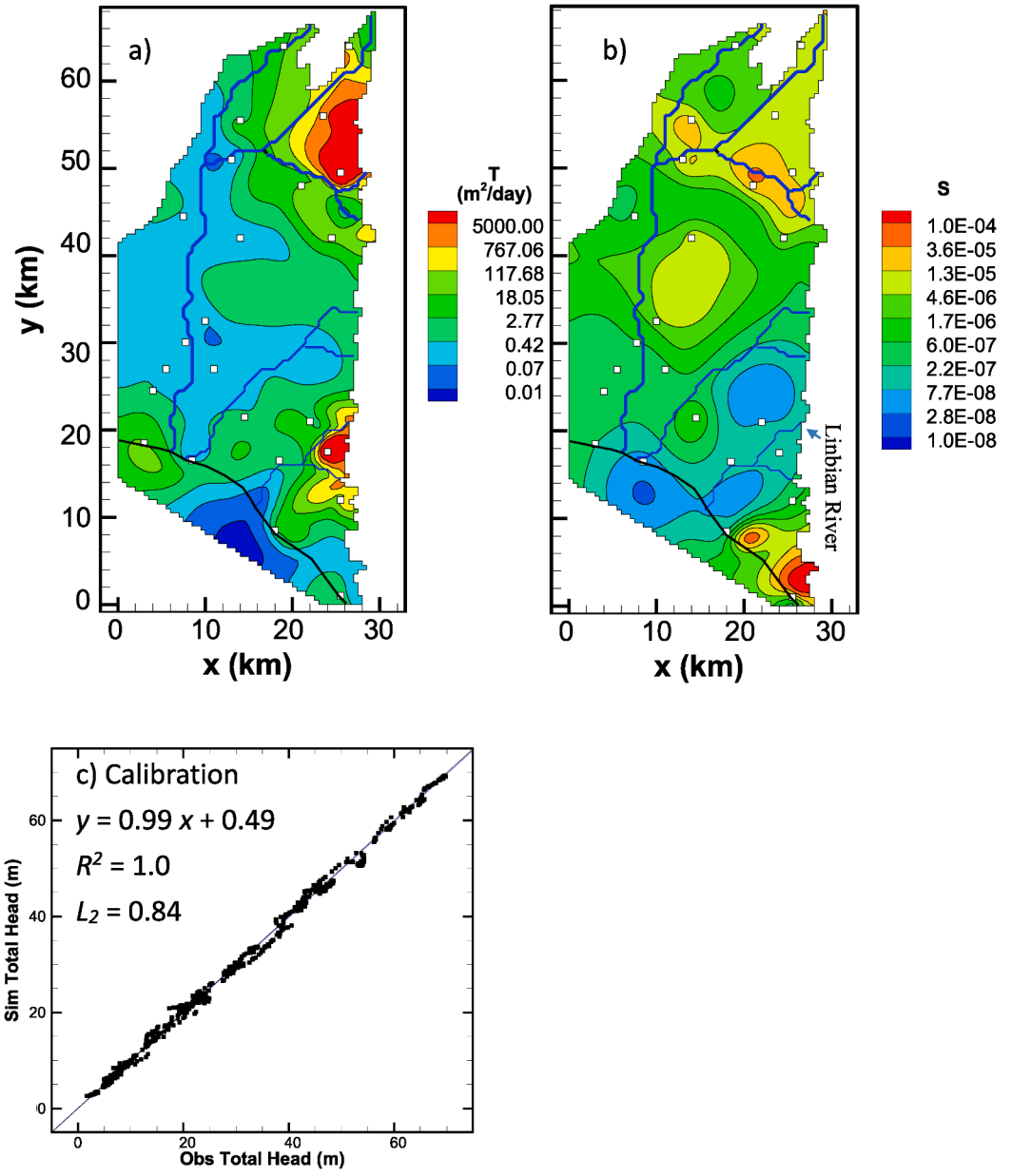

Fig. 5. The estimated a) hydraulic transmissivity T (m^2/day) and b) storage coefficient S fields based on uniform mean. c) The scatterplot of observed and calibrated groundwater levels. The white squares denote the wells where the groundwater levels were utilized to calibrate the model. Note that the groundwater levels from 23 (out of 35) wells between June to September 2006 are used to invert the parameter fields.

both the x and y directions for ln$T$ and ln$S$. Correlation scales represent the average size of the heterogeneity based on a visual analysis of the geological map (Fig. 1b). The estimates of variance and correlation lengths were imprecise, but their effects on the estimated T and S fields were minimized due to the large number of hydraulic data, which already carried information about the detailed site-specific heterogeneity.

5.2. Estimated T and S distributions based on uniform means

We inverted the parameter fields of the highly parameterized conceptual model, starting with uniform mean values for T and S across the entire aquifer. Fig. 5a and 5b display the estimated distributions for T and S, respectively, while Fig. 5c shows the scatterplot of observed and calibrated groundwater levels from 23 wells between June to September 2006. The scatterplot demonstrates excellent calibration as most groundwater levels are distributed along the 45-degree line, indicating a good agreement between the observed and simulated levels.

Fig. 5a shows that the estimated high T zones (red color) are primarily located in the upstream and mountain front regions near the northern and eastern boundaries, while the relatively low T zones (blue color) are in some areas of the middle plain and extend along the shoreline. The T patterns are consistent with the geological cross-sectional profiles based on core samples (Fig. 1b), where gravel deposits are concentrated in the upstream region, and fine sand and some silt/clay materials are primarily located along the coast. In addition, the relatively low T zone at the upper left-hand side of the plain (around x = 10 and y = 50) is consistent with the sand deposition (green color) in the same region in Fig. 1b. The large T values in the upstream and mountain front region correspond to the thick gravel deposition (greater than150 m thick). The estimated S field (Fig. 5b) follows a similar trend, except in regions near the upstream of the Linbian River. We observed that the estimated S values in this upstream region are relatively small (blue color near the right-hand side boundary), while the T values in the same area are high. This negative correlation was difficult to relate to the geology at this site. T values are typically positively correlated with S values in sedimentary deposition (Wang et al., 2022a) and negatively correlated with fractured geological media (Illman et al., 2009).

Next, we speculate that incorporating prior information about the general distributions of coarse-grained (e.g., gravel) and fine-grainded (e.g., sand and silt) material zones as starting T and S fields for river stage tomographic analysis may improve the estimates at the basin-scale site. This speculation is based on the usefulness of geological information at the meter-scale and kilometer-scale sites reported by Zhao and Illman (2017, 2018) and Zha et al. (2019). It would be interesting to investigate whether geological information at the basin-scale site is still helpful since the basin-scale geological profiles based on point-scale core samples likely have significant uncertainty.

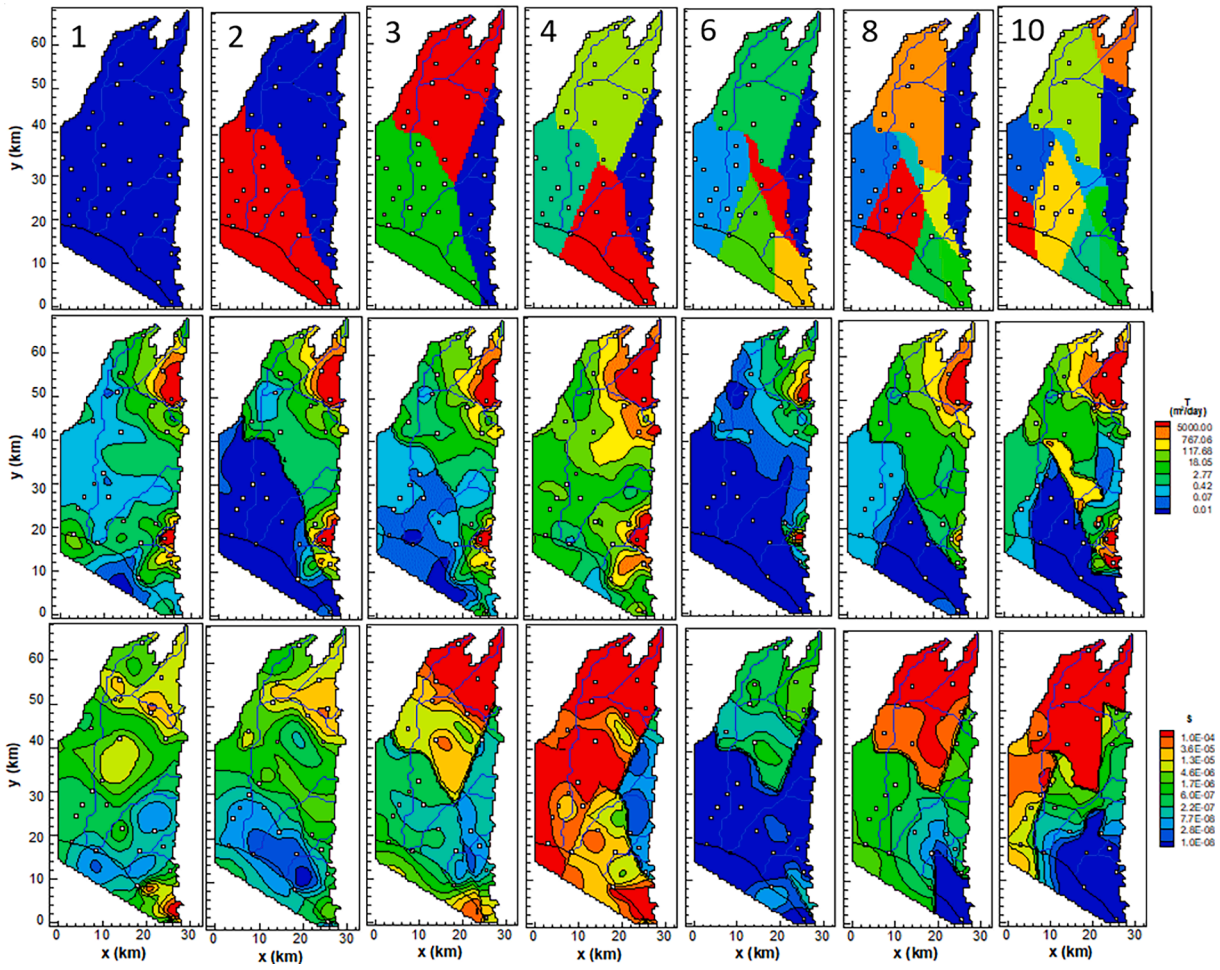

Fig. 6. The estimated hydraulic transmissivity T (m^2/day) and S fields with different number of zones as prior mean. The levels presented in the contour legends are identical to those in Fig. 5a and 5b. The numerals located in the upper left corner of the first row denote the quantity of zones. The white squares in the first row denote the wells where the geological information was utilized to create the zones. The white squares in the second and third rows denote the wells where the groundwater levels were utilized to calibrate the model.

5.3. Estimated T and S distributions based on calibrated zonal means

As mentioned, the estimated field from the zonation model was used as prior mean values for calibrating the parameter values of a highly parameterized conceptual model. The first row of Fig. 6 displays seven zonation geometries. The patterns of these zone models reflect the general geological structure of the site at different degrees (Fig. 1b). For the two-zone model, the boundary of zones roughly reflects the deposition of gravel (blue in Fig. 1b) and fine-grain materials (green and yellow in Fig. 1b). As the number of zones increased, the zone geometries further characterized each basin's upstream, midstream, and downstream.

The estimated T and S fields, using different numbers of zones as prior information, are illustrated in the second and third rows of Fig. 6. The time series of observed and calibrated groundwater levels with 4 prior mean zones are presented in Fig. 7 (Please refer to Fig. S2 for the scatterplots and Fig. S3-1 to S3-9 for the time series of different number of zones). These calibrated heads generally captured the correct trends, as the observed heads are within the range of uncertainty (i.e., one standard deviation). Fig. 8 summarized the calibrated head performances, including L_2, slope, intercept, and R^2, of the inversion as a function of the number of zones. Unlike the previous studies in the meter-scale and kilometer-scale sites (Zhao and Illman, 2017, 2018; Zha et al., 2019) who reported that the prior geological information improves the calibration performances, our inversion in a basin-scale site shows that the calibration performances remain similar when the number of zones is between 1 and 4. As the number of zones increases to more than 4, the L_2 and intercept deteriorate rapidly. This result may be

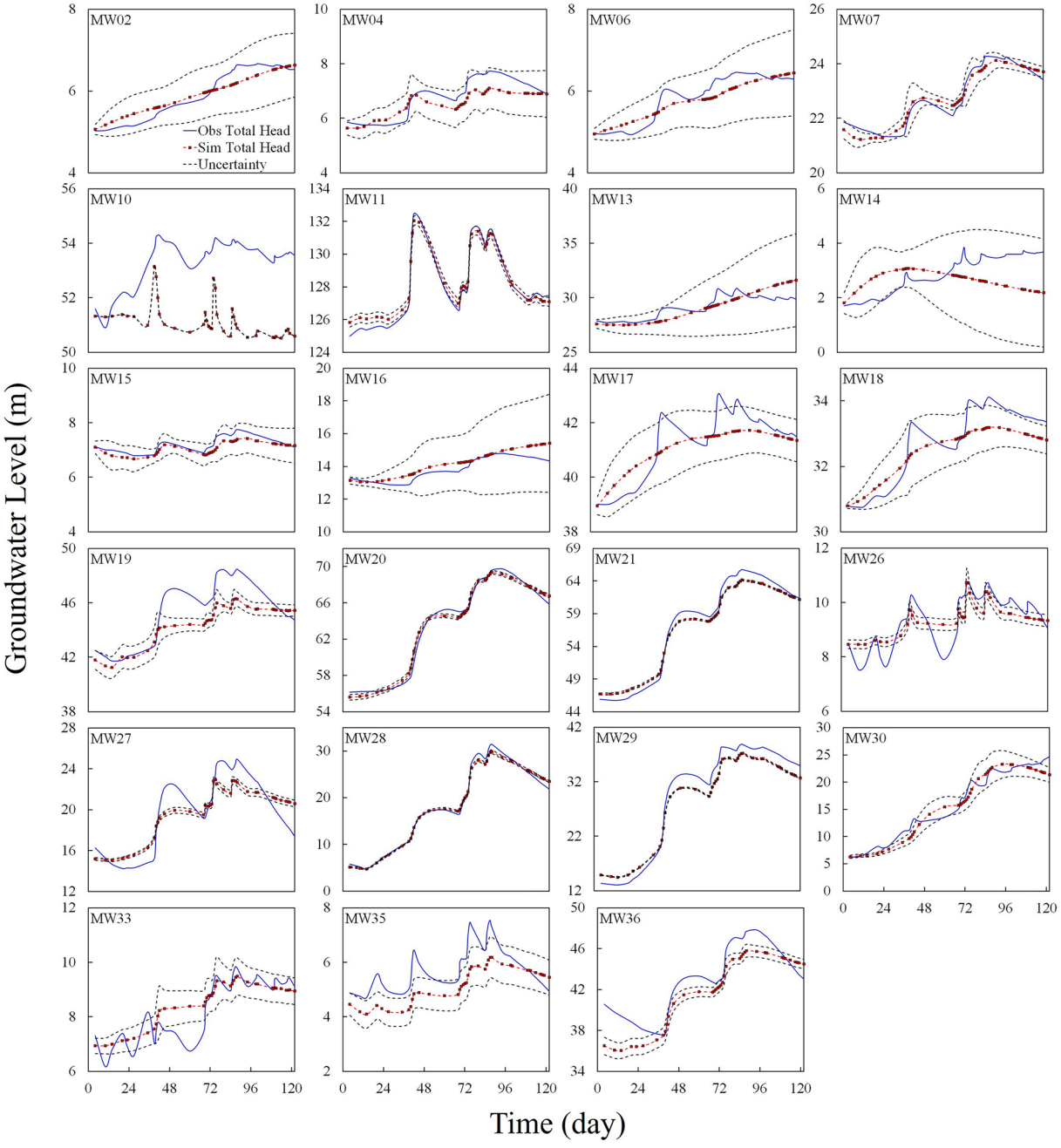

Fig. 7. The observed and calibrated groundwater levels with 4 prior mean zones. Please refer to Fig. S6 for the well locations. The red markers are the groundwater levels used to invert the parameter fields. The black dash lines are the uncertainty of simulated groundwater levels. It is estimated using the first order approximation (Eq. (7)).

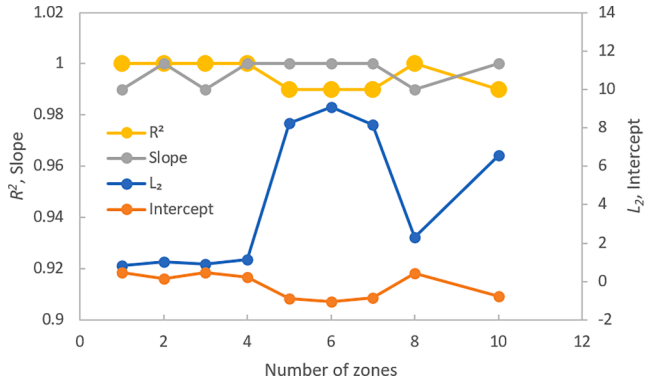

Fig. 8. The calibrated head performances (L_2, slope, intercept, and R^2) with different number of zones.

because the prior zone information is based on sparse point samples and limited soil types (i.e., gravel, sand, and silt/clay). While a few numbers of zones can capture the large-scale high T and low T (or S) information, the over-classification of clusters may misplace some regions in the wrong zone. In addition, previous studies have suggested that if the inversion is ill-defined (a common situation for most applications), the inversion using a highly parameterized model is sensitive to the initial parameter values (Illman et al., 2008; Wang et al., 2017; Liu et al., 2020). An inappropriate prior mean value can lead to over- or under-estimated parameter values or spurious anomalies.

Lastly, the estimated parameter fields were evaluated for their ability to predict independent head datasets (i.e., validation of the estimates). Fig. 9 compares the predicted groundwater levels to the actual values collected from 12 monitoring wells, excluded in the inversion, as a function of the number of zones. The time series of observed and validated groundwater levels with 4 prior mean zones are presented in Fig. 10 (Please refer to Fig. S4 for the scatterplots and Fig. S5-1 to S5-9 for the time series of different number of zones). The predicted heads generally captured the correct trend, as indicated by the slope and R^2 values close to 1. The L_2 values in the figure suggested that the geological data improved the estimates. As the number of zones increased from 1 to 3, the L_2 decreased by 62%. Further increasing the number of zones did not improve the validation, and even deteriorated the estimate when the number of zones exceeded 6, as indicated by the increasing discrepancies between the predicted and observed heads.

Overall, the geological information at the basin-scale site is still valuable, despite the uncertainties in the prior information of zones derived from sparse point samples and limited soil types since it captures the large-scale trends of hydraulic parameters. By selecting an appropriate number of zones, the calibrated geological clustering model can be a useful prior mean for highly parameterized models and improve the

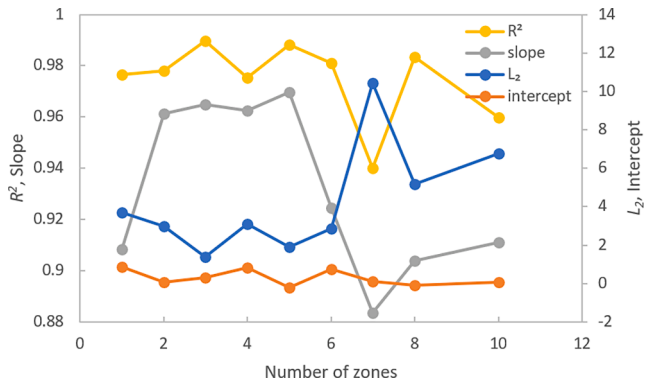

Fig. 9. The validated head performances (L_2, slope, intercept, and R^2) with different number of zones.

estimates.

6. Conclusions and future work

We analyzed the groundwater level responses induced by the variations of river stage due to the heavy rainfall events in a plain. These variations of groundwater levels exhibited different patterns, reflecting the heterogeneous nature of the aquifer at this site. We selected the data during wet seasons, which consist of six significant rainfall events.

Through the correlation analysis of stream stage and the corresponding groundwater level changes, we confirm that the groundwater levels likely carried non-redundant information about aquifer heterogeneity. These datasets were then analyzed using the geostatistical inverse code SLE to derive the spatial T and S distributions. These estimated fields corroborated with the geological model. Clustering schemes for deriving initial zonal mean T and S values for SLE to improve the estimates were examined. The impacts of the number of prior zones on the estimated T and S values were studied by validating the estimated field with the independent datasets not used in the calibration.

We conclude that integrating existing multiscale datasets, including the groundwater levels and point-scale geological information, by the appropriate scheme improves the inversion. Compared with the inversion using a uniform prior mean, the estimated fields with a few pre-calibrated zonal means lead to a better validation performance, while the calibration performance remains similar. This result stems from the fact that a few numbers of zones delineated based on the geological information, despite uncertainties of the zones derived from sparse point samples and limited soil types, can capture the large-scale trends of hydraulic parameters.

As the number of zones increases, the estimates deteriorate because the clustering does not consider hydrogeological processes such as sediment transport and deposition physics. With the classification solely based on the relative distance between the core samples and the limited number of soil types, the over-classification of clusters may misplace some regions in the wrong zone. For the study, pre-calibrated zonal mean with approximately three zones resulted in the best validation results.

The proposed method provides a cost-effective way for basin-scale characterization using existing monitoring networks. The stream stage and groundwater level monitoring records provide information on site hydrogeology that has largely been untapped. As unexpected droughts largely influence the water resources needs of every sector of the society, a systematic review of the historical hydrological records can save the investigation costs by deploying resources to regions requiring further refinement. The valuable insights into subsurface hydraulic heterogeneity can be used as evidence to support management decisions.

The future work can include joint inversion of head data and other information, such as hydraulic profiling tool (Zhao and Illman, 2022; Zhao et al., 2023), flowrate profiles (Tso et al., 2016), chemistry (Gumm et al., 2016; Mayer et al., 2007), groundwater age (Castro and Goblet, 2005; Marshall et al., 2020), and geophysical data (Tsai et al., 2017; Wang et al., 2022b). A 3-D groundwater model can also be used, as borehole logs are mainly used to delineate the vertical changes of subsurface heterogeneity. The borehole logs by nature should benefit the groundwater modeling most in refining the model in the vertical direction. In addition, the method to improve the S estimate needs further investigation. Lastly, we promote the vision of exploiting natural stimuli for characterizing basin-scale subsurface.

Declaration of Competing Interest

The authors declare that they have no known competing financial interests or personal relationships that could have appeared to influence the work reported in this paper.

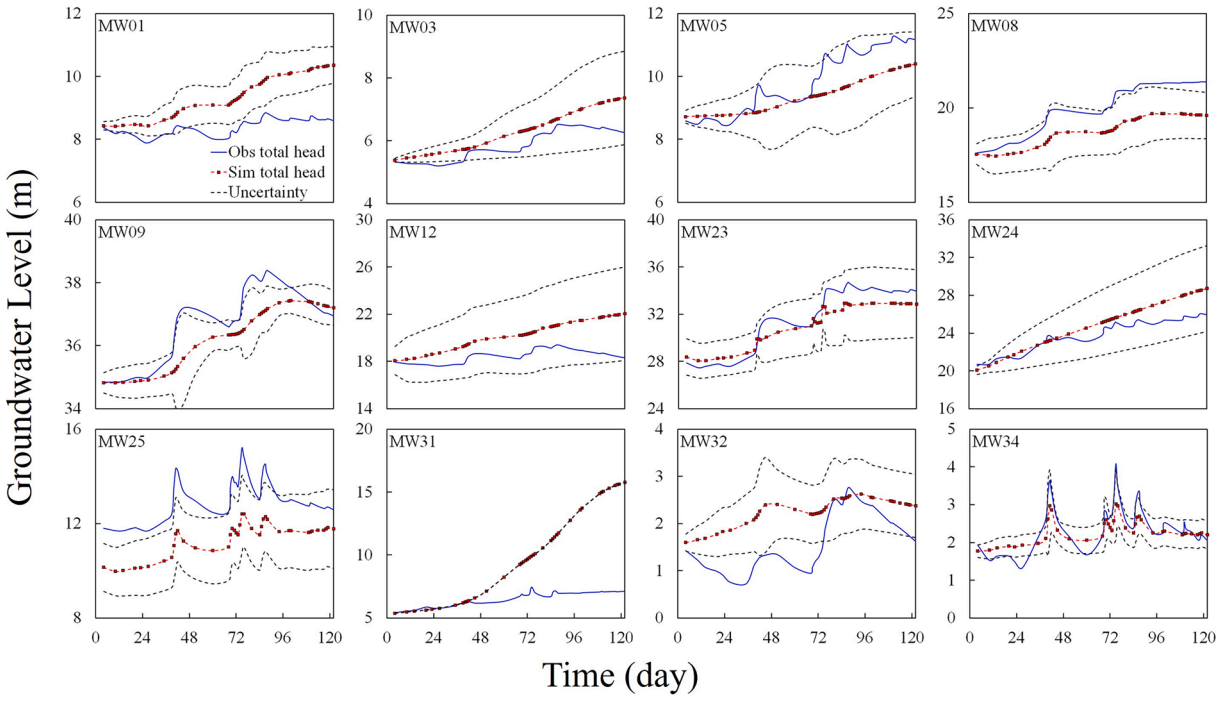

Fig. 10. The observed and validated groundwater levels with 4 prior mean zones. Please refer to Fig. S6 for the well locations. The red markers are the groundwater levels used to validate the parameter fields. The black dash lines are the uncertainty of simulated groundwater levels. It is estimated using the first order approximation (eq. (7)). (For interpretation of the references to color in this figure legend, the reader is referred to the web version of this article.)

Data availability

Data will be made available on request.

Acknowledgment

We would like to acknowledge the funding provided by the fund program for the scientific activities of selected returned overseas professionals in Shaanxi Province (No. 2020006) and Agricultural Net-Zero Carbon Technology and Management Innovation Research Center at National Taiwan University. We also gratefully acknowledge the supports of the following grants: TW NSC grants MOST111-2222-E-002-006, MOST110-2625-M-224-001, and MOST111-2625-M-224-001. The authors thank the editors and reviewers for their helpful and insightful comments, which have significantly improved the quality of this paper.

Appendix A. Supplementary data

Supplementary data to this article can be found online at https://doi.org/10.1016/j.jhydrol.2023.130061.

References

Arthur, D., Vassilvitskii, S., 2007. K-means++: The advantages of careful seeding. Proceedings of the 18th Annual ACM-SIAM Symposium on Discrete Algorithms. SIAM, pp. 1027–1035. https://doi.org/10.5555/1283383.1283494.

Bredehoeft, J., 2005. The conceptualization model problem—Surprise. Hydrgeol. J. 13 (1), 37–46. https://doi.org/10.1007/s10040-004-0430-5.

Cardiff, M., Kitanidis, P.K., 2009. Bayesian inversion for facies detection: An extensible level set framework. Water Resour. Res. 45, W10416. https://doi.org/10.1029/2008WR007675.

Castro, M.C., Goblet, P., 2005. Calculation of ground water ages—A comparative analysis. Groundwater 43 (3), 368–380. https://doi.org/10.1111/j.1745-6584.2005.0046.x.

Central Geological Survey, (1994). The geological map of Pingtun Plain, Minist. of Econ. Affairs, Taipei, Taiwan. https://twgeoref.moeacgs.gov.tw/GipOpenWeb/wSite/ct?xItem=120802&ctNode=1179&mp=106.

Enemark, T., Peeters, L.J.M., Mallants, D., Batelaan, O., 2019. Hydrogeological conceptual model building and testing: a review. J. Hydrol. 569, 310–329. https://doi.org/10.1016/j.jhydrol.2018.12.007.

Gumm, L.P., Bense, V.F., Dennis, P.F., Hiscock, K.M., Cremer, N., Simon, S., 2016. Dissolved noble gases and stable isotopes as tracers of preferential fluid flow along faults in the Lower Rhine Embayment, Germany. Hydrogeol. J. 24 (1), 99–108. https://doi.org/10.1007/s10040-015-1321-7.

Gupta, H.V., Clark, M.P., Vrugt, J.A., Abramowitz, G., Ye, M., 2012. Towards a comprehensive assessment of model structural adequacy. Water Resour. Res. 48, W08301. https://doi.org/10.1029/2011WR011044.

Hartmann, A., Gleeson, T., Wada, Y., Wagener, T., 2017. Enhanced groundwater recharge rates and altered recharge sensitivity to climate variability through subsurface heterogeneity. Environ. Sci. 114 (11), 2842–2847. https://doi.org/10.1073/pnas.1614941114.

Hoffman, F., 1993. Groundwater Remediation Using "Smart Pump and Treat". Groundwater 31, 98–106. https://doi.org/10.1111/j.1745-6584.1993.tb00833.x.

Hsiao, C.-T., Chang, L.-C., Tsai, J.-P., Chen, Y.-C., 2017. Features of spatiotemporal groundwater head variation using independentcomponent analysis. J. Hydrol. 547, 623–637. https://doi.org/10.1016/j.jhydrol.2017.02.021.

Iglesias, M.A., Lu, Y., Stuart, A.M., 2016. A Bayesian level set method for geometric inverse problems. Interfaces Free Bound. 18 (2), 181–217. https://doi.org/10.4171/IFB/362.

Illman, W.A., Craig, A.J., Liu, X., 2008. Practical issues in imaging hydraulic conductivity through hydraulic tomography. Groundwater 46 (1), 120–132. https://doi.org/10.1111/j.1745-6584.2007.00374.x.

Illman, W.A., Liu, X., Takeuchi, S., Yeh, T.-C.-J., Ando, K., Saegusa, H., 2009. Hydraulic tomography in fractured granite: Mizunami Underground Research site, Japan. Water Resour. Res. 45, W01406. https://doi.org/10.1029/2007WR006715.

Jafarzadeh, A., Khashei-Siuki, A., Pourreza-Bilondi, M., 2022. Performance assessment of model averaging techniques to reduce structural uncertainty of groundwater modeling. Water Resour. Manag. 36, 353–377. https://doi.org/10.1007/s11269-021-03031-x.

Jardani, A., Dupont, J.P., Revil, A., Massei, N., Fournier, M., Laignel, B., 2012. Geostatistical inverse modeling of the transmissivity field of a heterogeneous alluvial aquifer under tidal influence. J. Hydrol. 472–473, 287–300. https://doi.org/10.1016/j.jhydrol.2012.09.031.

Lee, J., Kitanidis, P.K., 2013. Bayesian inversion with total variation prior for discrete geologic structure identification. Water Resour. Res. 49, 7658–7669. https://doi.org/10.1002/2012WR013431.

Liu, N., Oliver, D.S., 2005. Ensemble Kalman filter for automatic history matching of geologic facies. J. Pet. Sci. Eng. 47 (3–4), 147–161. https://doi.org/10.1016/j.petrol.2005.03.006.

Liu, F., Yeh, T.-C.J., Wang, Y.-L., Hao, Y., Wen, J.-C., Wang, W., 2020. Characterization of basin-scale aquifer heterogeneity using transient hydraulic tomography with aquifer responses induced by groundwater exploitation reduction. J. Hydrol. 588, 125–137. https://doi.org/10.1016/j.jhydrol.2020.125137.

Luo, N., Zhao, Z., Illman, W.A., Berg, S.J., 2017. Comparative study of transient hydraulic tomography with varying parameterizations and zonations: Laboratory sandbox investigation. J. Hydrol. 554, 758–779. https://doi.org/10.1016/j.jhydrol.2017.09.045.

Luo, N., Illman, W.A., Zha, Y., 2022. Large-scale three-dimensional hydraulic tomography analyses of long-term municipal wellfield operations. J. Hydrol. 610, 127911 https://doi.org/10.1016/j.jhydrol.2022.127911.

Marshall, S.K., Cook, P.G., Konikow, L.F., Simmons, C.T., Dogramaci, S., 2020. Conjoint use of hydraulic head and groundwater age data to detect hydrogeologic barriers. Hydrogeol. J. 28 (3), 1003–1019. https://doi.org/10.1007/s10040-019-02095-9.

Mayer, A., May, W., Lukkarila, C., Diehl, J., 2007. Estimation of fault-zone conductance by calibration of a regional groundwater flow model: Desert Hot Springs, California. Hydrogeol. J. 15 (6), 1093–1106. https://doi.org/10.1007/s10040-007-0158-0.

Michael, H.A., Khan, M.R., 2016. Impacts of physical and chemical aquifer heterogeneity on basin-scale solute transport: vulnerability of deep groundwater to arsenic contamination in Bangladesh. Adv. Water Resour. 98, 147–158. https://doi.org/10.1016/j.advwatres.2016.10.010.

Promma, K., Zheng, C., Asnachinda, P., 2007. Groundwater and surface-water interactions in a confined alluvial aquifer between two rivers: Effects of groundwater flow dynamics on high iron anomaly. Hydrgeol. J. 15 (3), 495–513. https://doi.org/10.1007/s10040-006-0110-8.

Refsgaard, J.C., Christensen, S., Sonnenborg, T.O., Seifert, D., Højberg, A.L., Troldborg, 2012. Review of strategies for handling geological uncertainty in groundwater flow and transport modelling. Adv. Water Resour. 36, 36–50. https://doi.org/10.1016/j.advwatres.2011.04.006.

Ramirez-Hernandez, J., Hinojosa-Huerta, O., Peregrina-Llanes, M., Calvo-Fonseca, A., Carrera-Villa, E., 2013. Groundwater responses to controlled water releases in the Limitrophe region of the Colorado River: Implications for management and restoration. Ecol. Eng. 59, 93–103. https://doi.org/10.1016/j.ecoleng.2013.02.016.

Sarris, T.S., Kenny, A., Scott, D.M., Close, M.E., 2022. Aquifer heterogeneity controls to quality monitoring network performance for the protection of groundwater production wells. Water Res. 218, 118485 https://doi.org/10.1016/j.watres.2022.118485.

Schöniger, A., Illman, W.A., Wöhling, T., Nowak, W., 2015. Finding the right balance between groundwater model complexity and experimental effort via Bayesian model selection. J. Hydrol. 531, 96–110. https://doi.org/10.1016/j.jhydrol.2015.07.047.

Sophocleous, M.A., 1991. Stream-floodwave propagation through the Great Bend alluvial aquifer, Kansas: Field measurements and numerical simulations. J. Hydrol. 124 (3–4), 207–228. https://doi.org/10.1016/0022-1694(91)90015-A.

Sun, N.-Z., Yeh, W. W.-G., 1990. Coupled inverse problems in groundwater modeling: 1. Sensitivity analysis and parameter identification. Water Resour. Res. 26 (10), 2507–2525. https://doi.org/10.1029/WR026i010p02507.

Sykes, J.F., Wilson, J.L., Andrews, R.W., 1985. Sensitivity analysis for steady-state groundwater flow using adjoint operators. Water Resour. Res. 21 (3), 359–371. https://doi.org/10.1029/WR021i003p00359.

Troldborg, L., Refsgaard, J.C., Jensen, K.H., Engesgaard, P., 2007. The importance of alternative conceptual models for simulation of concentrations in a multi-aquifer system. Hydrgeol. J. 15, 843–860. https://doi.org/10.1007/s10040-007-0192-y.

Tsai, J.-P., Yeh, T.-C.-J., Cheng, C.-C., Zha, Y., Chang, L.-C., Hwang, C., Wang, Y.-L., Hao, Y., 2017. Fusion of time-lapse gravity survey and hydraulic tomography for estimating spatially varying hydraulic conductivity and specific yield fields. Water Resour. Res. 53, 8554–8571. https://doi.org/10.1002/2017WR020459.

Tso, C.-H.M., Zha, Y., Yeh, T.-C.J., Wen, J.-C., 2016. The relative importance of head, flux, and prior information in hydraulic tomography analysis. Water Resour. Res. 52, 3–20. https://doi.org/10.1002/2015WR017191.

Wang, Y.-L., Yeh, T.-C.J., Wen, J.-C., Huang, S.-Y., Zha, Y., Tsai, J.-P., Hao, Y., Liang, Y., 2017. Characterizing subsurface hydraulic heterogeneity of alluvial fan using riverstage fluctuations. J. Hydrol. 547, 650–663. https://doi.org/10.1016/j.jhydrol.2017.02.032.

Wang, Y.-L., Chang, L.-C., Liu, F., Ho, Y.-T., Wang, T.B., Yeh, T.-C.-J., Tsai, J.-P., 2022a. Aquifer Characterization Using Fiber Bragg Grating Multi-Level Monitoring System. Groundwater 60, 518–529. https://doi.org/10.1111/gwat.13186.

Wang, Y.-L., Yeh, T.-C.J., Liu, F., Wen, J.-C., Wang, W., Hao, Y., 2022b. Characterize basin-scale subsurface using rocket-triggered lightning. Geophys. Res. Lett. 49, e2022GL101278 https://doi.org/10.1029/2022GL101278.

Wang, Y.-L., Yeh, T.-C.J., Wen, J.-C., Gao, X., Zhang, Z., Huang, S.-Y., 2019. Resolution and ergodicity issues of river stage tomography with different excitations. Water Resour. Res. 55, 4974–4993. https://doi.org/10.1029/2018WR023204.

Xiang, J., Yeh, T.-C.J., Lee, C.-H., Hsu, K.-C., Wen, J.-C., 2009. A simultaneous successive linear estimator and a guide for hydraulic tomography analysis. Water Resour. Res. 45, W02432. https://doi.org/10.1029/2008WR007180.

Yeh, T.-C.J., Dong, Y., Ye, S., 2023. An Introduction to Solute Transport in Heterogeneous Geologic Media. Cambridge University Press, Cambridge. https://doi.org/10.1017/9781009049511.

Yeh, T.-C.J., Jin, M., Hanna, S., 1996. An iterative stochastic inversemethod: Conditional effective transmissivity and hydraulic head fields. Water Resour. Res. 32 (1), 85–92. https://doi.org/10.1029/95WR02869.

Yeh, T.-C.J., Lee, C.-H., Hsu, K.-C., Illman, W.A., Barrash, W., Cai, X., Daniels, J., Sudicky, E.d., Wan, L.i., Li, G., Winter, C.L., 2008. A view toward the future of subsurface characterization: CAT scanning groundwater basins. Water Resour. Res. 44 (3) https://doi.org/10.1029/2007WR006375.

Yeh, T.-C.J., Xiang, J., Suribhatla, R.M., Hsu, K.-C., Lee, C.-H., Wen, J.-C., 2009. Riverstage tomography: A new approach for characterizing groundwater basins. Water Resour. Res. 45, W05409. https://doi.org/10.1029/2008WR007233.

Yen, B.C., Tsai, C.-W.-S., 2001. On noninertia wave versus diffusion wave in flood routing. J. Hydrol. 244 (1–2), 97–104. https://doi.org/10.1016/S0022-1694(00)00422-4.

Zha, Y., Yeh, T.-C.J., Illman, W.A., Mok, C.M.W., Tso, C.-H.-M., Carrera, B.A., Wang, Y.-L., 2019. Exploitation of pump-and-treat remediation systems for characterization of hydraulic heterogeneity. J. Hydrol. 573, 324–340. https://doi.org/10.1016/j.jhydrol.2019.03.089.

Zhang, Y., Schaap, M.G., Guadagnini, A., Neuman, S.P., 2016. Inverse modeling of unsaturated flow using clusters of soil texture and pedotransfer functions. Water Resou. Res. 52, 7631–7644. https://doi.org/10.1002/2016WR019016.

Zhao, Z., Illman, W.A., Berg, S.J., 2016. On the importance of geological data for hydraulic tomography analysis: Laboratory sandbox study. J. Hydrol. 542, 156–171. https://doi.org/10.1016/j.jhydrol.2016.08.061.

Zhao, Z., Illman, W.A., 2017. On the importance of geological data for three-dimensional steady-state hydraulic tomography analysis at a highly heterogeneous aquifer-aquitard system. J. Hydrol. 544, 640–657. https://doi.org/10.1016/j.jhydrol.2016.12.004.

Zhao, Z., Illman, W.A., 2018. Three-dimensional imaging of aquifer and aquitard heterogeneity via transient hydraulic tomography at a highly heterogeneous field site. J. Hydrol. 559, 392–410. https://doi.org/10.1016/j.jhydrol.2018.02.024.

Zhao, Z., Illman, W.A., 2022. Integrating hydraulic profiling tool pressure logs and hydraulic tomography for improved high-resolution characterization of subsurface heterogeneity. J. Hydrol. 610, 127971 https://doi.org/10.1016/j.jhydrol.2022.127971.

Zhao, Z., Luo, N., Illman, W.A., 2023. Geostatistical analysis of high-resolution hydraulic conductivity estimates from the hydraulic profiling tool and integration with hydraulic tomography at a highly heterogeneous field site. J. Hydrol. 617, 129060 https://doi.org/10.1016/j.jhydrol.2023.129060.